1. Introduction and literature review

1.1. Introduction

1.1.1. Overview of neurodegenerative diseases (NDDs): demography and epidemiology

The term "neurodegeneration" describes the progressive loss of a neuron's structure and/or functions, which might include death [1]. Neurodegeneration is a broad category of illnesses that mainly affect the elderly and have a big influence on people's health as well as the health of society. Age is the primary demographic factor influencing neurodegeneration. Neurodegenerative diseases include Alzheimer's disease (AD), Parkinson's disease (PD), Huntington's disease (HD), and amyotrophic lateral sclerosis (ALS), and are characterized by the gradual loss of structure or function of neurons, leading to cognitive and motor impairments [2].

Dementia is the biggest global health concern, which is characterized by a decline in cognitive function that affects memory, thinking, behavior, and the ability to do daily tasks. As per the latest data, there are already 69 million dementia patients worldwide. This number is expected to rise to 82 million by 2030 and 152 million by 2050 as the population ages [3]. Our risk of dementia increases with age. At any given time, 5-8 % of people aged 60 and beyond suffer from dementia. Women are disproportionately affected, perhaps due to their longer life expectancy. For instance, more than two-third of the population affected with Alzheimer's disease, the most common kind of dementia, are female **(Figure 1.1**).

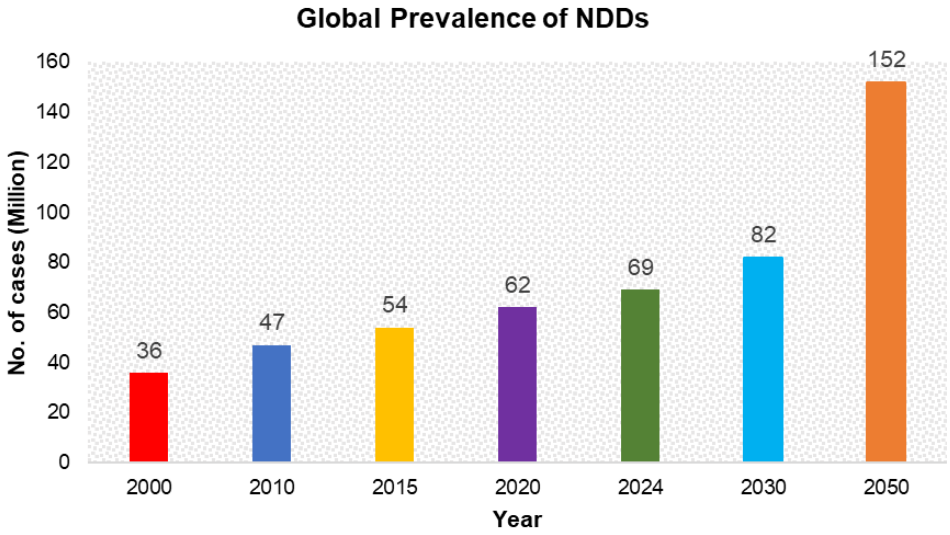

Figure 1.1. Global prevalence of NDDs and their future predicted estimate

1.1.2. Overview of NDDs

Based on clinical presentations, neurodegenerative diseases are broadly classified as cognitive or behavioral disorders followed by extrapyramidal and pyramidal movement disorders. The majority of patients have mixed clinical characteristics, with very few having pure symptoms. Proteotoxic stress and its associated abnormalities in the ubiquitin–proteasomal and autophagosomal/lysosomal systems, oxidative stress, programmed cell death, and neuroinflammation are among the fundamental processes linked to progressive neuronal dysfunction and death, even though neurodegenerative diseases are usually characterized by specific protein accumulations and anatomic vulnerability [4, 5].

Amyloidoses, tauopathies, α-synucleinopathies, and transactivation response DNA binding protein 43 (TDP-43) proteinopathies are the most prevalent forms of neurodegenerative diseases [6]. The primary histopathological characteristics necessary for establishing a particular neuropathological diagnosis in these illnesses are abnormal protein conformations and their distribution in cells and neurons. Tau in neurofibrillary tangles (NFTs) or Pick bodies, α-synuclein in Lewy bodies, and TDP-43 in neuronal cytoplasmic and neuronal intranuclear inclusions are a few examples of protein accumulations within

neurons. Tau in tufted astrocytes, astrocytic plaques, and thorn-shaped astrocytes are examples of protein accumulations found inside astrocytes [7].

Accumulated proteins in oligodendroglia include Tau in coiled bodies and α-synuclein in glial cytoplasmic inclusions. The protein frequently exhibits an aberrant structure with characteristics similar to those of amyloid plaques. Their secondary structures are richer in β-pleated sheets and the majority form filaments. Many protein aggregates, including amyloid plaques, NFTs, and a subpopulation of lewy bodies, can be identified using amyloid stains like Congo red and thioflavin S; however, silver-staining techniques are more effective in identifying other aggregates. Due to its superior interlaboratory and inter-rater reliability, immunohistochemistry is currently the method of choice for researching neurodegenerative diseases.

There are several factors such as abnormalities in protein dynamics resulting in the generation of reactive oxygen species (ROS), oxidative stress, aggregation and misfolding of protein, altered bioenergetics, mitochondrial dysfunction (proteinopathy), impaired biometal homeostasis (copper, iron and zinc), and the formation of free radicals. Furthermore, amyloid oligomer biomarkers like amyloid-β and α-synuclein cause impairment in the cellular and mitochondrial membrane permeability along with the above-mentioned factors [8]. Neurodegeneration is generally caused by irreversible progressive damage to the brain neurons. There are several problems associated with body parts movement (ataxia), cognitive function (dementia), learning, memory and behavior in the aged population. The pathological abnormalities that arise from the above factors result in Alzheimer's disease (AD), Parkinson's disease (PD), Huntington's disease (HD), multiple sclerosis (MS), motor neuron disease, and prion's disease. AD is the most common type of dementia and accounts for about 70-80 % of total cases. AD shares clinical hallmark features *viz.* extracellular senile plaque (deposits of polymorphous β-amyloid protein) and

intracellular neurofibrillary tangles (formed by hyperphosphorylation of microtubule-associated protein tau) as well as brain atrophy (**Figure 1.2**). There are several target hypotheses for the pathological progression of the disease including the cholinergic hypothesis, oxidative stress hypothesis, neuroinflammatory hypothesis, β-amyloid hypothesis, and metal ion hypothesis. Each hypothesis has a separate set of steps of pathogenesis but finally meets the same goal of neuronal damage. The multifaceted nature of neurodegeneration has provided a ground to researchers where they can impart their drug-designing skills to come up with such a molecule bearing multiple pharmacophoric scaffolds for different target proteins.

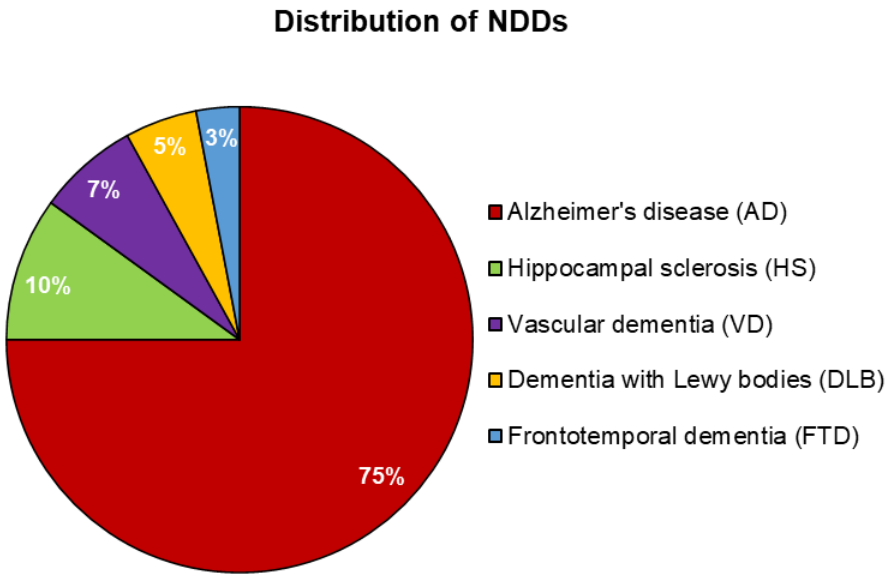

Figure 1.2. Pie chart showing the distribution of neurodegenerative diseases

1.1.2.1. Alzheimer's disease

A mixed type of proteinopathy is observed in the neuropathology of AD that includes the occurrence of Aβ deposits in the parenchyma as amyloid or senile plaques and neuronal tau inclusions (i.e., NFTs). Neuronal processes (also known as "dystrophic neurites"), as well as both astroglial processes and microglia, are among the diverse cellular components of amyloid plaques. When thick deposits are present, microglia are especially common. Tau-

immunoreactive dystrophic neurites, or "neuritic plaques," are the most clinically relevant kind of plaque in AD.

For the neuropathological diagnosis of AD, the topographic distribution of NFTs and the density of neuritic plaques is required. There are several target hypotheses (cholinergic, dopaminergic, oxidative stress, NMDA, metal ions hypothesis, etc.) for the formation of β-amyloid plaques (Aβ), NFTs and progression of disease in AD patients [9]. The cholinergic hypothesis indicates the role of AChE in the progression of AD. AChE degrades acetylcholine (ACh), a key neurotransmitter that works in the cognitive function of the brain. A high level of AChE has been observed in AD patients along with decreased level of ACh [10]. Studies show that AChE available in neuronal cells binds with amyloid plaque and increases its neurotoxicity [11]. On the other hand, depletion of dopamine levels in the brain is one of the leading causes of AD and is mediated by oxidative stress. Dopamine is metabolized by monoamine oxidase (MAO), and reduced dopamine level causes cognitive impairment while oxidative stress leads to neuronal damage [12, 13]. Thus, NDDs are multifaceted in nature and different cellular mechanisms are attributed to their pathogenesis.

The multitarget-directed ligands (MTDLs) approach has emerged as a potential design strategy for targeting NDDs of multifactorial origin [14]. In recent years, MTDL campaigns have produced several small molecules with multitarget inhibitory potential against monoamine oxidases (MAO-A and B), cholinesterases (AChE and BChE), beta-secretase-1 (BACE1) and β-amyloid (Aβ) peptide aggregation, etc. Particularly, MAOs and ChEs are the widely explored targets for the discovery of novel MTDLs for the treatment of NDDs [15, 16]. The well-known multifunctional ligands, rivastigmine and ladostigil act by inhibiting AChE-BChE and MAO-B-AChE enzymes, respectively.

Monoamine oxidases (MAOs) are flavin adenine dinucleotide (FAD) containing outer mitochondrial membrane-bound enzymes that exist in two isoforms viz. MAO-A and MAO-B. These isoforms share nearly 70 % sequence homology and contain 527 and 520 amino acid residues, respectively. MAOs catalyze the oxidative deamination of biogenic monoamine neurotransmitters to corresponding aldehyde, ammonia, and hydrogen peroxide. The C-terminal α-helix domain of both the isoforms acts as an anchoring point and provides attachment with the outer mitochondrial membrane, N-terminal domain binds with FAD whereas the central domain forms an active site for the binding of monoamine substrate [17]. The active site of MAO-A is slightly larger than that of MAO-B due to which it catalyzes the deamination of substrates larger than dopamine (serotonin and noradrenaline). The MAO-B has two cavities in its active site, the first of which is termed as the entrance cavity having a volume of ~290 $Å^3$, and the second cavity known as the substrate cavity having a volume of ~390 $Å^3$. Both entrance and substrate cavities are connected by the Ile199 side-chain and it serves as a gate [18]. The cofactor, FAD lies at the end of the substrate cavity near which a favorable amine binding region is formed by parallel tyrosyl residues (Tyr398 and Tyr435) and is termed an aromatic cage [19]. Based on the substrate specificity, MAO-A is a potential therapeutic target for anxiety and depression whereas MAO-B is a potential target for AD and PD therapy [20, 21].

The anomaly in the homeostasis of ACh is due to the hyperactivity of two cholinesterases; AChE and butyrylcholinesterase (BChE). AChE is primarily expressed in the brain neurons, while BChE is mainly expressed in the glial cells and acts as a compensatory part in the hydrolysis of ACh [15]. Both AChE and BChE share about 65 % sequence similarity and are encoded by separate genes. A catalytic triad formed by Ser203, Glu334, and His447 residues hydrolyzes acetylcholine. Apart from ACh hydrolysis, the peripheral anionic site (PAS) of AChE is found to promote aggregation of β-amyloid plaque which is neurotoxic

and promotes neuroinflammation and apoptosis (**Figure 1.3**) [22, 23]. Further, impaired metal ion homeostasis in the brain plays a significant role in the progression of AD and other NDDs. Among the three metal ions (Fe^{++}, Cu^{++} and Zn^{++}), iron plays a principal role in the metabolism of neurotransmitters and other cellular functions [24]. Iron catalyzes the production of reactive oxygen species (ROS) by participating in the Fenton reaction which results in further aggregation of neurotoxic β-amyloid plaques and mitochondrial oxidation [25]. Thus, MTDLs possessing iron-chelation capabilities can be beneficial in addressing iron-mediated neurological complications.

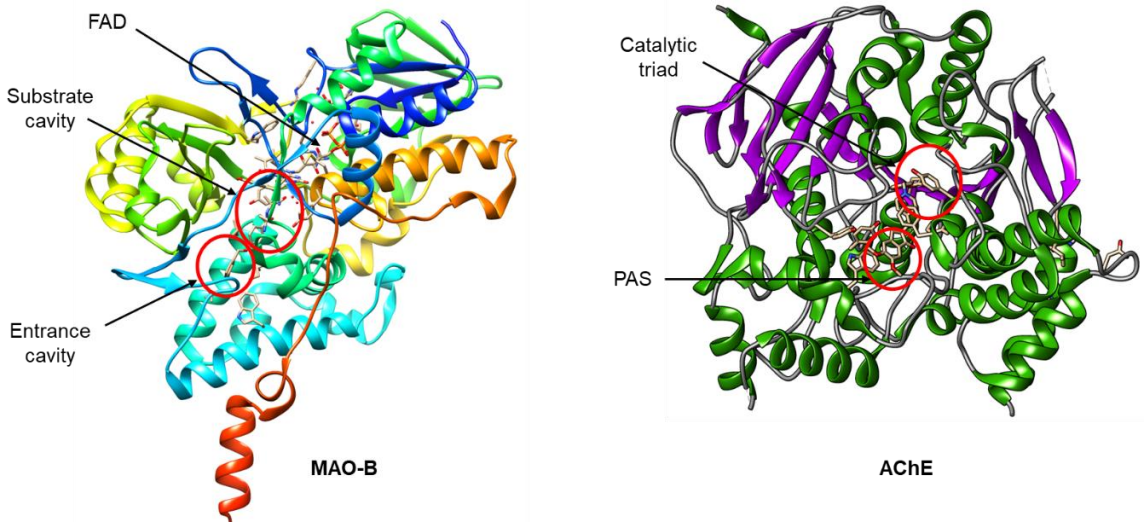

Figure 1.3. Protein structure of target enzymes MAO-B and AChE; red circles in MAO-B indicate entrance cavity and substrate cavity while in AChE red circle indicates peripheral anionic site and catalytic triad in the active site.

1.1.2.2. Parkinson's disease

Parkinson's disease (PD) is a prevalent neurodegenerative condition that includes a variety of clinical hallmarks and non-motor symptoms such as bradykinesia, resting tremor, rigidity, and later developing postural instability. Although the exact etiology of Parkinson's disease is unknown, various genetic risk factors and genes that produce uncommon family variants of the disease have recently been identified. Intracellular aggregates of α-synuclein, which are the pathological hallmark of the movement disorder, are caused by the death of dopaminergic neurons in the substantia nigra pars compacta (SNpc) [26].

Alpha-synuclein (α-syn) is a protein that plays a role in regulating synaptic activity and neurotransmitter release in the brain. The majority of native α-synuclein in the brain is unfolded and lacks a defined tertiary structure; nonetheless, it can exist as stable tetramers that are resistant to aggregation in aqueous solutions [27]. When α-synuclein interacts with negatively charged lipids, like the phospholipids found in cell membranes, its N-terminal folds into α-helical structures. A β-sheet-rich, amyloid-like form that is prone to aggregation is adopted by α-synuclein in Parkinson's disease.

One important factor in the pathophysiology of both familial and idiopathic Parkinson's disease is thought to be mitochondrial malfunction. An essential part of the electron transport chain, the mitochondrial complex-I, was shown to be lacking in the SNpc of PD brains in early postmortem investigations [28].

1.1.3. Neuroprotectants and their role in treating various NDDs

The term ‘neuroprotection’ refers to the strategies and mechanisms applied to protect the neurons of the central nervous system (CNS) against acute (CNS trauma and brain stroke) and chronic (neuronal diseases like Alzheimer’s disease, Parkinson’s disease, and multiple sclerosis, etc.) neuronal damage caused by various environmental factors and neurodegenerative disorders. The neuronal cell's defense against various threats, such as ROS-induced cellular damage, elevated hydrogen peroxide, reduced SOD, and chemical neurotoxins, either through internal neuroprotective systems like glutathione peroxidase or external drug molecules or antioxidants. There are various types of neuroprotectants, including drugs, antioxidants, and natural compounds along with nerve growth factors, anti-inflammatory agents, free radical scavengers, and hormones.

Neuroprotective agents play a crucial role in either the prevention of neuronal damage due to neuroinflammation and apoptosis or the management of pathological conditions

resulting from injury and damage of nerve cells. Neuroprotective agents produce their action through one or more mechanisms.

1.2. Literature review

Development of small molecule multitarget-directed ligands (MTDLs) capable of simultaneously inhibiting two different protein targets is an emerging and promising approach for treating complex neurodegenerative disorders. The most widely explored dual targets include MAOs and ChEs, β-amyloid (Aβ) and ChEs, Aβ and β-site amyloid precursor cleaving enzyme 1 (BACE1), ChEs and BACE1, ChEs and BACE1, BACE1 and Tau, ChEs and FAAH, ChEs, and NMDA, ChEs, and tau, Aβ and tau etc., exploited for MTDL design, especially for NDDs [29-38]. Simultaneous inhibition of these pairs of targets in general offers superior efficacy and therapeutic benefits than selective or single target inhibition.

During the last decade, a large number of small molecules have been reported as potent dual MAO-AChE inhibitors. The design of such inhibitors is primarily based on the emerging MTDL approach wherein the pharmacophores of MAO and AChE inhibitory activity are fused in a single molecule. We summarize and highlight below the structure and activity profile of diverse classes of fused MTDL hybrids (**Table 1.1**) and other synthetic (**Table 1.2**) and natural (**Table 1.3**) dual MAO-AChE inhibitors reported during the last decade.

1.2.1. Synthetic hybrids of available drugs as dual MAO-AChE inhibitors

There are several synthetic small molecule hybrids of available single target drugs and active synthon or natural scaffold reported by different research groups claiming potent inhibitory activity against dual MAO and ChE enzymes along with some auxiliary activities. These hybrids include tacrine-PF9601N, tacrine-selegiline, tacrine-coumarin, coumarin-dithiocarbamate, coumarin-benzylpiperidine and donepezil-butylated

hydroxytoluene (BHT) hybrid. Additionally, donepezil-indolyl, donepezil-propargylamine-8-hydroxyquinoline hybrids, donepezil-trolox hybrids, and pyridoxine-resveratrol hybrids have been designed and evaluated for their dual MAO-ChE inhibitory properties. The structure and multifunctional profile of developed MTDL hybrids are summarized in **Table 1.1**.

Table 1.1. Structure and activity profile of reported dual MAO-AChE inhibitory MTDL hybrids

SN	Structure	MAO IC_{50} (μM)	ChE IC_{50} (μM)	Additional activities	Reference
1.	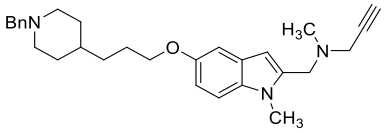	MAO-A 0.005 ± 0.001 μM Irreversible type MAO-B 0.043 ± 0.008 μM Irreversible type	*hr*AChE 0.380 ± 0.050 μM Mixed type *h*BChE 1.700 ± 0.200 μM	Aβ-aggregation	[39]
2.	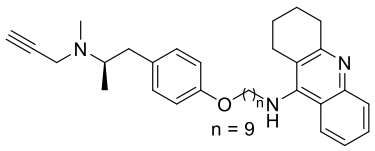	*h*MAO-A 0.372 ± 0.025 μM *h*MAO-B 0.181 ± 0.030 μM Irreversible type	*ee*AChE 0.023 ± 0.003 μM Mixed type *eq*BChE 0.009 ± 0.001 μM	-	[40]
3.	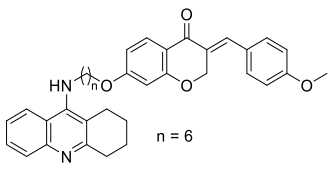	MAO-B 0.401 ± 0.011 μM Irreversible type	*ee*AChE 0.068 ± 0.004 μM Mixed type *eq*BChE 0.033 ± 0.003 μM	PAMPA-BBB	[41]
4.	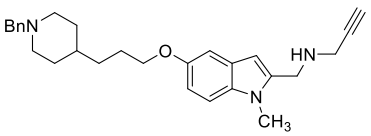	*h*MAO-A 0.006 ± 0.001 μM *h*MAO-B 0.150 ± 0.031 μM	*ee*AChE 0.190 ± 0.010 μM Mixed type *eq*BChE 0.830 ± 0.160 μM	QSAR	[42]
5.	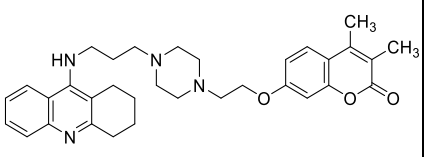	*h*MAO-A 15.07 ± 0.88 μM *h*MAO-B 0.240 ± 0.010 μM Reversible type	*ee*AChE 0.034 ± 0.001 μM Mixed type *eq*BChE 0.081 ± 0.002 μM	PAMPA-BBB, SH-SY5Y toxicity	[43]

6.	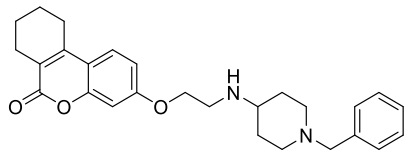	*h*MAO-B 2.620 ± 0.810 µM Reversible type	*h*AChE 1.370 ± 0.050 µM Mixed type hBChE 1.980 ± 0.080 µM	PAMPA-BBB, Hepatotoxicity HepG2, SH-SY5Y toxicity	[44]
7.	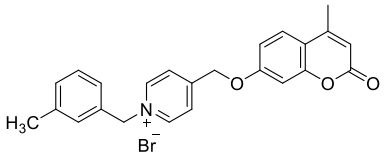	hMAO-B 1.570 ± 0.050 µM	*h*AChE 0.084 ± 0.004 µM *eq*BChE 2.320 ± 0.200 µM	Aβ-aggregation SH-SY5Y toxicity	[45]
8.	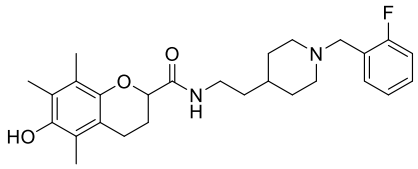	*h*MAO-A 4.400 ± 0.200 µM *h*MAO-B 4.300 ± 0.200 µM	*ee*AChE 0.310 ± 0.030 µM *eq*BChE 3.910 ± 0.110 µM	Aβ-aggregation, PC12, HepG-2, BV-2 toxicity, DPPH, Cu^{2+} chelation, acute toxicity in mouse	[46]
9.	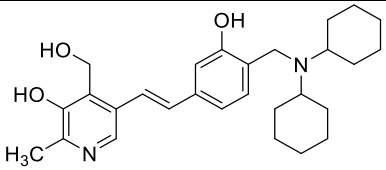	*hr*MAO-B 12.400 ± 0.360 µM	*ee*AChE 2.110 ± 0.100 µM Mixed type	Antioxidant, metal chelation	[47]
10.	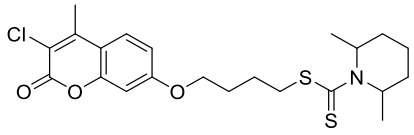	*h*MAO-B 0.101 ± 0.024 µM Reversible type	*ee*AChE 0.044 ± 0.002 µM Mixed type	PAMPA-BBB, SH-SY5Y toxicity, *in vivo* neuroprotection, acute toxicity	[48]
11.	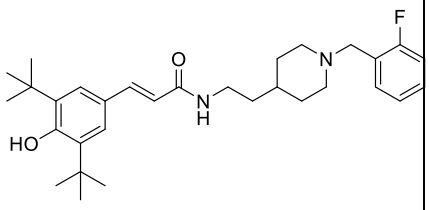	*h*MAO-B 7.400 ± 0.200 µM	*ee*AChE 0.075 ± 0.050 µM Mixed type	PAMPA-BBB, Aβ-aggregation, PC12, DPPH, BV-2, rat liver microsomes stability, *in vivo* neuroprotection	[49]
12.	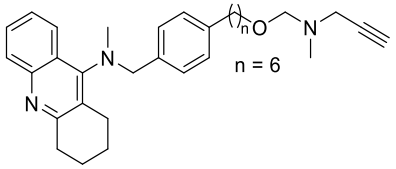	*h*MAO-A 2.300 ± 0.030 µM *h*MAO-B 4.75 ± 0.240 µM	*h*AChE 4.840 ± 0.450 µM *h*BChE 0.610 ± 0.050 µM	PAMPA-BBB, PC12, BV-2 toxicity, *in vivo* acute toxicity, *in vivo* pharmacokinetic study	[50]

1.2.2. Synthetic small molecule dual MAO-AChE inhibitors

Several synthetic small molecule inhibitors of MAO and ChE have been reported to possess dual inhibitory potential and multitarget inhibition profiles. These molecules consist of

different kinds of chemical scaffolds which play a vital role in the biological activity towards a particular target while some of the scaffolds have the potential to exert potent inhibitory activity on more than one target. Coumarin is a natural scaffold that possesses potent MAO inhibitory activity while propargyl moiety selectively increases MAO-B inhibition (selegiline) [51]. Benzylpiperidine is a known scaffold present in donepezil (a selective AChE inhibitor) and is reported to increase the potency of the molecule towards AChE when included in its template [52]. Benzodioxole moiety is reported to possess dual MAO-AChE inhibitory activity. Apart from this, several naturally occurring compounds have benzodioxole moiety such as berberine, avicine, sesamol, machilin A, myristicin, dillapiole, apiole, and safrole which have neuroprotective potential and are employed in the design of novel small molecule potent inhibitors [53]. The structure and multifunctional profile of various classes of synthetic MTDLs are summarized in **Table 1.2**.

Table 1.2. Structure and activity profile of reported synthetic dual MAO-AChE inhibitors

SN	Structure	MAO IC_{50} (µM)	ChE IC_{50} (µM)	Additional activities	Reference
1.	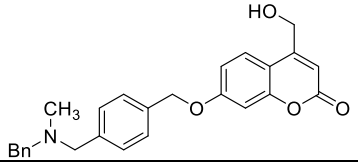	*hr*MAO-B 0.010 ± 0.002 µM	*hr*AChE 0.120 ± 0.010 µM Mixed type	PAMPA-BBB, SH-SY5Y	[51]
2.	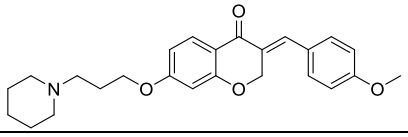	*hr*MAO-B 3.440 ± 0.040 µM Irreversible type	*ee*AChE 3.940 ± 0.050 µM Mixed type	-	[54]
3.	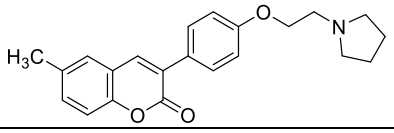	*h*MAO-A 1.570 ± 0.080 µM hMAO-B 0.064 ± 0.002 µM	*h*AChE 0.195 ± 0.007 µM *h*BChE 28.200 ± 1.300 µM	Aβ-aggregation, antioxidant, PAMPA-BBB, PC12,	[55]
4.	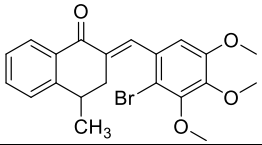	*r*MAO-A 0.920 ± 0.120 µM rMAO-B 0.880 ± 0.120 µM	AChE 0.045 ± 0.020 µM BChE 12.500 ± 1.100 µM	Aβ-aggregation, PC12 toxicity, PC12 neuroprotection	[56]
5.	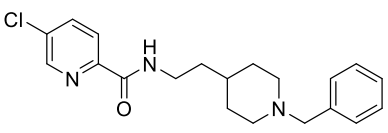	*h*MAO-A 13.40 ± 0.900 µM *h*MAO-B 3.140 ± 0.270 µM	*ee*AChE 0.220 ± 0.006 µM Mixed type *eq*BChE 1.230 ± 0.100 µM	Metal chelation (Cu^{2+}), PAMPA-BBB, PC12 toxicity	[52]

6.	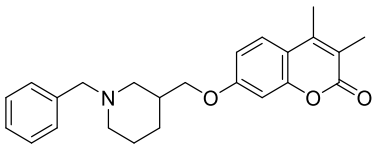	*hr*MAO-A 2.810 ± 0.800 µM *hr*MAO-B 0.030 ± 0.005 µM	*ee*AChE 1.030 ± 0.030 µM Mixed type *eq*BChE 3.410 ± 0.190 µM	SH-SY5Y toxicity, Transport across MDCKII-MDR1 Cells	[57]
7.	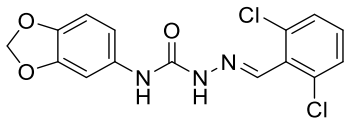	*r*MAO-A 4.52 ± 0.032 µM *r*MAO-B 0.059 ± 0.002 µM Competitive reversible	*r*AChE 0.0087 ± 0.0002 µM Mixed type reversible	-	[16]
8.	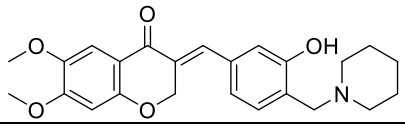	*hr*MAO-B 1.740 ± 0.058 µM	*ee*AChE 0.003 ± 0.0001 µM Mixed type	Aβ-aggregation, Metal chelation (Cu^{2+}), PAMPA-BBB, PC12 toxicity	[58]
9.	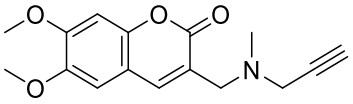	*r*MAO-B 0.003 ± 0.0004 µM	*ee*AChE 8.990 ± 0.500 µM	SH-SY5Y toxicity, SH-SY5Y neuroprotection, Transport across MDCKII-MDR1 Cells	[59]
10.	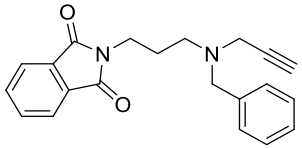	*h*MAO-B 2.600 ± 0.050 µM	*h*AChE 1.20 ± 0.070 µM Mixed type *h*BChE 3.80 ± 0.080 µM	PAMPA-BBB, SH-SY5Y toxicity	[60]
11.	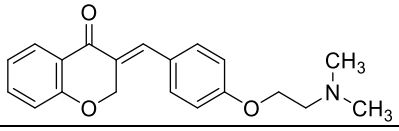	*h*MAO-B 0.037 ± 0.0002 µM noncompetitive	*h*AChE 0.657 ± 0.002 µM Mixed type	PAMPA-BBB, *in vivo* neuroprotection	[61]
12.	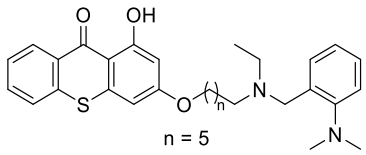	MAO-A 1.010 ± 0.020 µM MAO-B 0.900 ± 0.010 µM	*ee*AChE 0.590 ± 0.020 µM Mixed type *eq*BChE 28.70 ± 0.540 µM	Aβ-aggregation, antioxidant, metal chelation (Cu^{2+}, Zn^{2+}, Fe^{2+} and Al^{3+}), PAMPA-BBB, SH-SY5Y	[62]
13.	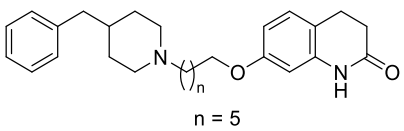	*hr*MAO-A 0.30 ± 0.001 µM hrMAO-B 1.40 ± 0.010 µM	*ee*AChE 0.560 ± 0.010 µM Mixed type *eq*BChE 2.300 ± 0.010 µM	PAMPA-BBB, PC12	[63]
14.	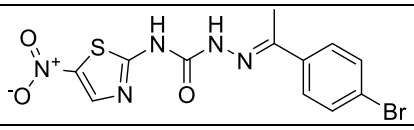	*r*MAO-B 0.212 ± 0.004 µM	*r*AChE 0.340 ± 0.007 µM	-	[64]
15.	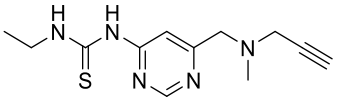	*r*MAO-B 1.427 ± 0.272 µM	*r*AChE 0.324 ± 0.022 µM	Aβ-aggregation, Antioxidant, metal chelation (Cu^{2+}, Zn^{2+}, Fe^{2+}), PAMPA-BBB, neuroprotection in primary cortical neuron, *in vivo* neuroprotection	[65]
16.	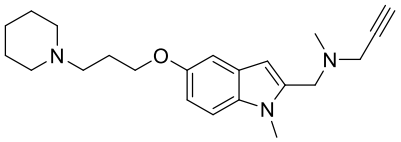	*h*MAO-A 0.145 µM *h*MAO-B 0.078 µM	*h*AChE 0.53 µM *h*BChE 1.69 µM	-	[66]

17.	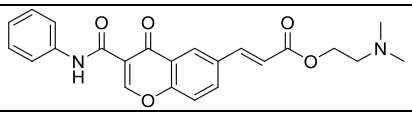	*h*MAO-B 0.630 ± 0.010 μM	*h*AChE 3.690 ± 0.240 μM *h*BChE 4.320 ± 0.290 μM	hBACE-1, PAMPA-BBB, SH-SY5Y toxicity, HepG2	[67]
18.	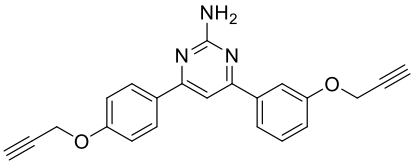	*h*MAO-B 1.49 ± 0.090 μM Reversible type	*ee*AChE 1.740 ± 0.070 μM Reversible type	metal chelation (Cu^{2+}, Fe^{2+}), SH-SY5Y toxicity & neuroprotection	[68]
19.	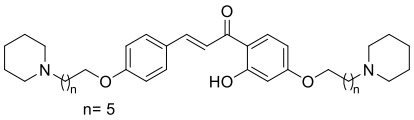	*hr*MAO-B 0.570 ± 0.010 μM	*h*AChE 0.780 ±0.020 μM	Aβ-aggregation, Antioxidant, metal chelation (Cu^{2+}, Zn^{2+}, Fe^{2+}), PC12 neuroprotection	[69]
20.	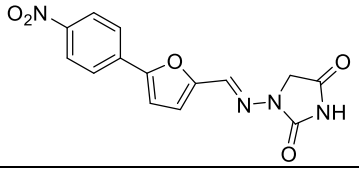	*hr*MAO-B 2.69 ± 0.440 μM	*h*AChE 4.19 ± 0.73 μM	Aβ-aggregation, DPPH Antioxidant, SH-SY5Y neuroprotection	[70]
21.	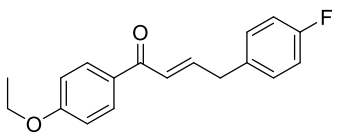	*hr*MAO-A 4.63 ± 0.150 μM *hr*MAO-B 0.053 ± 0.003 μM Competitive reversible type	*hr*AChE 20.6 ± 0.150 μM	-	[71]
22.	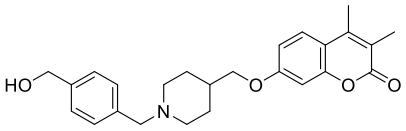	*hr*MAO-A 1.40 ± 0.30 μM *hr*MAO-B 0.029 ± 0.0080 μM	*ee*AChE 1.00 ± 0.070 μM *eq*BChE 8.80 ± 1.40 μM	SH-SY5Y neuroprotection	[72]
22.	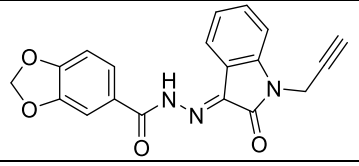	*r*MAO-A 1.73 ± 0.087 μM *r*MAO-B 0.034 ± 0.007 μM Competitive reversible type	*r*AChE 0.85 ± 0.107 μM Competitive reversible type *r*BChE 0.88 ± 0.007 μM	-	[73]
23.	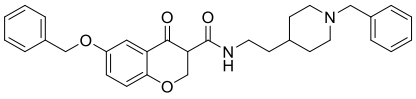	*hr*MAO-B 0.035 ± 0.003 μM Competitive inhibitor	*hr*AChE 1.85 ± 0.160 μM Competitive inhibitor	PAMPA-BBB, PC12 toxicity	[74]
24.	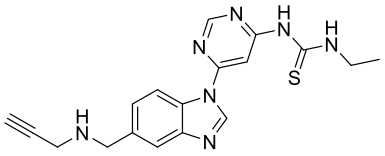	*h*MAO-B 2.117 ± 0.061 μM	*m*AChE 0.032 ± 0.007 μM	Aβ-aggregation, PAMPA-BBB, metal chelation, Antioxidant, *in vivo* neuroprotection	[75]
25.	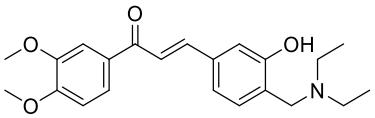	MAO-B 1.21 ± 0.030 μM	*ee*AChE 0.44 ± 0.040 μM	Aβ-aggregation, Antioxidant, metal chelation (Cu^{2+}, Zn^{2+}, Fe^{2+} and Al^{3+})	[76]
26.	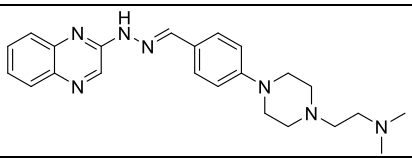	*h*MAO-B 0.046 ± 0.002 μM	AChE 0.028 ± 0.001 μM	-	[77]
27.	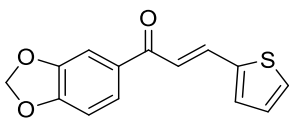	*hr*MAO-A 0.023 ± 0.003 μM *hr*MAO-B 0.026 ± 0.0019 μM Reversible type	*hr*AChE 9.57 ± 1.02 μM	PAMPA-BBB	[78]

28.	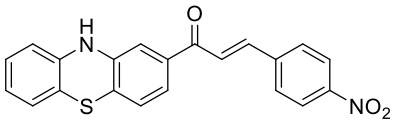	*h*MAO-B 0.048 ± 0.001 μM	*ee*AChE 0.053 ± 0.001 μM	-	[79]
29	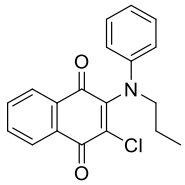	*h*MAO-B 0.054 ± 0.001 μM	*ee*AChE 3.50 ± 0.30 μM	Aβ-aggregation, PAMPA-BBB	[80]
30.	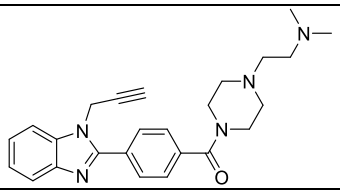	*h*MAO-B 0.041 ± 0.002 μM Reversible-noncompetitive	AChE 0.024 ± 0.001 μM Reversible and mixed-type	Aβ-aggregation	[81]
31.	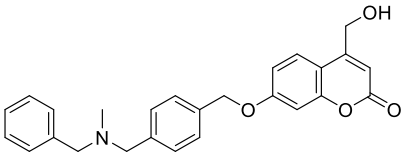	*h*MAO B 0.010 ± 0.002 μM	*h*AChE 0.12 ± 0.01 μM	-	[82]
32.	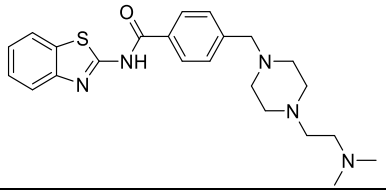	MAO-B 0.040 ± 0.002 μM	AChE 0.023 ± 0.001 μM	Aβ aggregation	[83]
33.	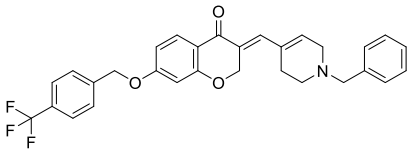	MAO-B 0.410 ± 0.040 μM	*ee*AChE 0.58±0.05 μM	Aβ aggregation	[84]
34.	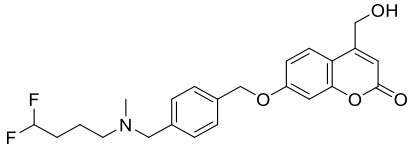	*h*MAO-B 0.008 ± 0.002 μM	*h*AChE 0.55 ± 0.07 μM	PAMPA-BBB assay	[29]
35.	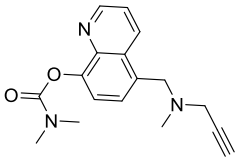	MAO-A 0.008 ± 0.001 μM MAO-B 7.90 ± 1.34 μM	AChE 0.52 ± 0.07 μM BChE 44.90 ± 6.10 μM	Aβ aggregation	[85]
36.	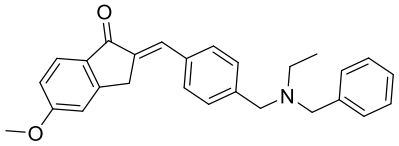	*h*MAO-B 0.355 ± 0.134 μM	*h*AChE 0.039 ± 0.001 μM *h*BChE 7.00 ± 0.01 μM	-	[86]
37.	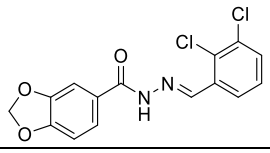	MAO-B 0.95 ± 0.12 μM non-competitive and reversible inhibition	AChE 0.048 ± 0.007 μM Reversible inhibition BChE 0.89 ± 0.018 μM	-	[15]

38.	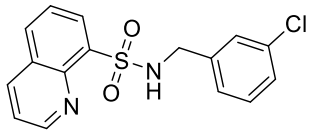	MAO-A 0.59 ± 0.04 µM MAO-B 0.73 ± 0.08 µM competitive.	AChE 1.95 ± 1.07 µM BChE 2.84 ± 1.07 µM competitive.	PAMPA-BBB	[87]
39.	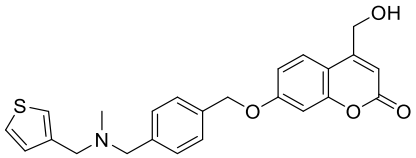	*h*MAO-B 0.015 ± 0.002 µM	*h*AChE 0.261 ± 0.071 µM *h*BChE 6.73 ± 0.23	PAMPA-BBB	[88]
40.	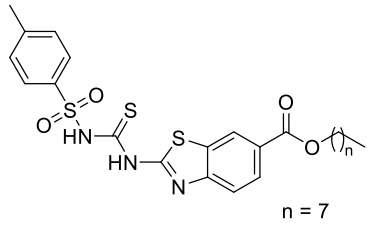	MAO-A 0.353 ± 0.010 µM Competitive inhibition MAO-B 0.716 ± 0.02 µM	*h*AChE 0.027 ± 0.008 µM competitive inhibition hBChE 0.043 ± 0.004 µM	-	[89]

1.2.3. Natural small molecule inhibitors of MAO-AChE

There have been several natural small molecules identified that possess dual MAO and AChE inhibitory properties (**Table 1.3**). Passos *et al.*, identified indole alkaloids from *Psychotria sp.* which contains dual MAO-ChE inhibition potential [90]. Sadaoui *et al.,* identified perillaldehyde from essential oil of Algerian *Ammodaucus leucotrichus* that exhibit dual MAO-ChE inhibitory activity [91]. Plazas *et al.*, isolated isoquinoline alkaloids from roots of *Zanthoxylum rigidum* which displayed potent multitarget potential against MAO-ChE inhibition and Aβ aggregation [92]. Oh *et al.*, identified ellagic acid derivatives from *Castanopsis cuspidata* var. *sieboldii* possessing dual MAO-ChE inhibitory activity [93].

Table 1.3. Structure and activity profile of reported natural dual MAO-AChE inhibitors

SN	Structure	MAO IC_{50} (µM)	ChE IC_{50} (µM)	Additional activities	Reference
1.	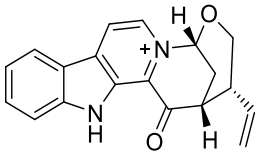	MAO-A 6.92 µM MAO-B 81 µM	AChE 3.39 µM noncompetitive BChE 11 µM	-	[90]
2.	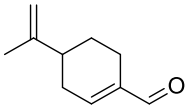	MAO-A 159.1 ± 25.9 µg/mL MAO-B 98.9 ± 7.2 µg/mL	AChE >1000 µg/mL BChE 42.7 ± 4.8 µg/mL	-	[91]

3.	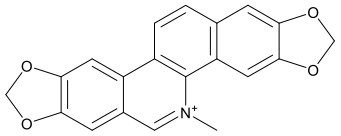	MAO-A 0.410 ± 0.020 µM MAO-B >100 µM	*ee*AChE 0.150 ± 0.010 µM Mixed type eqBChE 0.880 ± 0.080 µM	Aβ aggregation	[92]
4.	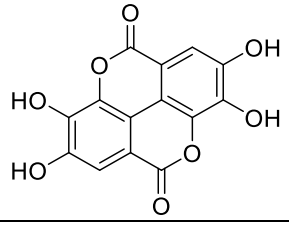	MAO-A >40 µM MAO-B 9.21 ± 0.16 µM Competitive type	AChE 41.7 ± 2.4 µM Mixed type BChE >40 µM	BACE-1, MDCK cell toxicity	[93]

1.2.4. Summary

A survey and review of current and available literature on NDDs and dual/multitarget inhibitors of MAO and ChEs revealed the following points:

- NDDs are high-prevalence CNS disorders with delayed diagnosis, limited treatment options, and low survival rates.
- There are several disease targets for the treatment, but dual MAO and ChE inhibition can produce better therapeutic outcomes due to the effect on other associated factors (oxidative stress and protein aggregation are related to high levels of MAO and AChE, respectively).
- There is considerable similarity in the active site of both enzymes (e.g., both have a volume of ~700 $Å^3$, and the active sites of both enzymes are rich in tyrosine).
- Several small molecule MAO and ChE inhibitors have been identified and most of the potent molecules among them contain a natural scaffold such as coumarin, benzodioxole, etc.

Based on the above inference, we employed a rational drug design approach and available appropriate protocols for the discovery of new small molecule dual MAOs-ChEs inhibitors and evaluated their *in vitro* and *in vivo* efficacy for neuroprotection.

1.3. Rationale, objectives and plan of work

1.3.1. Rationale and design strategy

Acetamides have a general formula of R_1-CH_2-CO-NH-R_2 and are known to possess several biological activities depending on the attached moiety (R_1 & R_2). Several phenylacetamides have been reported to exhibit good inhibitory potential against cholinesterase enzymes [94, 95]. Apart from cholinesterase inhibition, acetamide derivatives have been identified to possess antidepressant, antioxidant, anti-cancer, analgesic and anti-inflammatory activity [96].

Small molecules possessing hydrazone (R-NH-N=C<R'R'') moiety are a stable, adaptable, and readily accessible class of compounds with a wide range of bioactivities, including analgesic, antimicrobial, antimalarial, antitumor, anticonvulsant, anti-inflammatory, antimycobacterial, and anti-HIV properties, as well as antidepressants and MAO inhibitory activity [97, 98]. The structural similarities of the MAO substrate, which primarily consists of amino/imino groups, can be used to explain the MAO inhibitory potential of hydrazone derivatives. They are essential for the ligand's binding to the MAO active site. Analogs of hydrazines (R-NH-NH_2), hydrazones are produced by condensing hydrazine with active carbonyl systems and have an azomethine (R-NH-N=CH-R') group. The hydrazone scaffold's physicochemical and biological characteristics are greatly influenced by the double bond in the C=N and/or NH group. The imino C-atom exhibits both nucleophilic and electrophilic characteristics, whereas the nitrogen in the hydrazone is nucleophilic. Additionally, carbohydrazones (R_1-CO-NH-N=CH-R_2) that are produced from carbohydrazides (R-CO-NH-NH_2) have a variety of biological properties, and other bioactive structural analogs have been derived by utilizing the carbonyl (R_1) and imino terminal (R_2) of the carbohydrazone moiety. Because of the aforementioned unique chemical characteristics, recent research has found several substituted carbohydrazones as

AChE and MAO inhibitors, making them a prospective framework for developing new MTDLs to treat CNS illnesses [99].

Benzodioxole is a well-established chemical scaffold that possesses several biological activities along with dual MAO-ChE inhibitory potential. A natural product containing benzodioxole moiety can produce molecules with reduced toxic effects and improved desired biological profile. The natural compound sesamol isolated from sesame seeds and sesame oil (*Sesamum indicum* L.), itself is a proven antioxidant and also possesses neuroprotective activity [100-106]. Besides sesamol, eugenol is also a natural product obtained mainly from clove oil and is well known for its analgesic and anti-inflammatory activity. In addition, eugenol is also reported to exhibit a neuroprotective effect on different disease models [107-114]. Eugenol has several other biological activities including antioxidant, antimicrobial, and anticancer activity (**Figure 1.4**).

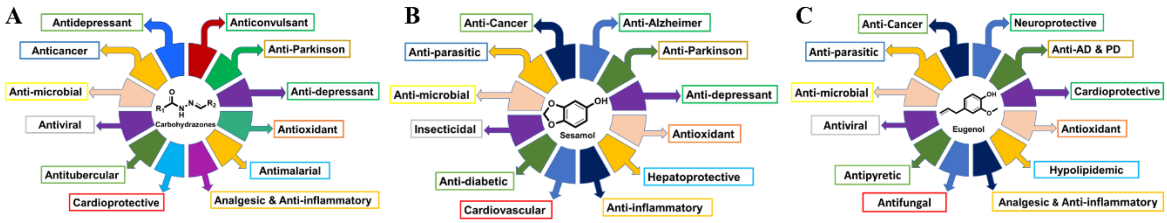

Figure 1.4. Biological activity profile of carbohydrazones (A), sesamol (B) and eugenol (C) derivatives

1.3.2. Objectives

Encouraged by the potent bioactivity profile of acetamides, carbohydrazones, sesamol and eugenol scaffolds we envisaged designing new molecular architectures by ligand/pharmacophore-guided hybridization and exploiting their multifunctional properties using a systematic drug discovery workflow (**Figure 1.5**). The major objectives of thesis work include:

- To develop a pharmacophore model using safinamide for the identification of a new MAO-B inhibitory scaffold through pharmacophore-based virtual screening.

- To design a library of virtual lead-based analogs and synthesize them using the retrosynthetic approach.
- To perform *in vitro* biological evaluation of synthesized compounds against MAOs (MAO-A/B) and ChEs (AChE and BChE) and antioxidant, metal chelation and PAMPA-BBB penetration assay of selected compounds.
- To evaluate the lead compound(s) for their *in vitro* cellular neurotoxicity and neuroprotective potential using the SH-SY5Y cell line.
- Molecular docking, computational prediction of dual MAO/ChE ligand binding efficiency, ADMETox property prediction of synthesized ligands and molecular dynamic simulation studies of selected molecule.
- *In vivo* evaluation (behavioral & acute toxicity assays) of lead dual MAO/ChE inhibitors.

1.3.3. Plan of work

To achieve the aforementioned objectives, a systematic research workflow was devised by combining multiple *in silico*, *in vitro* and *in vivo* methodologies. A complete schematic diagram for the proposed workflow is presented in **Figure 1.5**.

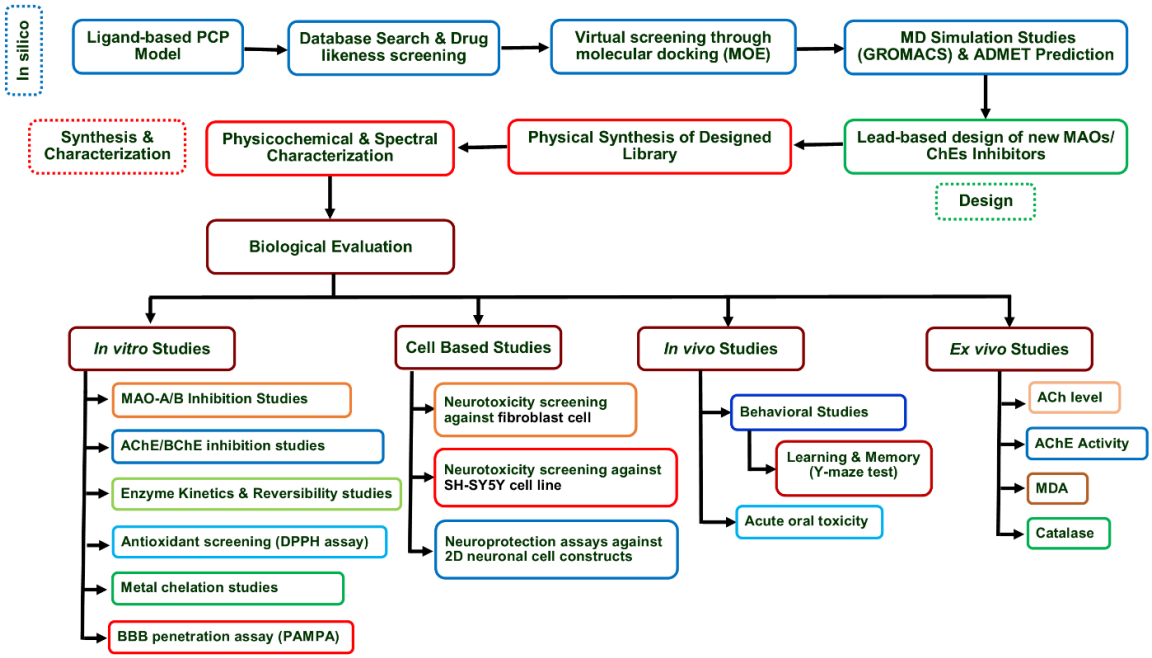

Figure 1.5. Schematic representation of comprehensive plan of work